Article

Excitation and Propagation of Guided Waves in Multilayer Hollow Cylinders Using PWAS Transducers: A Theoretical and Experimental Study

Roshan Joseph *, **Lingyu Yu, Victor Giurgiutiu**

Department of Mechanical Engineering, University of South Carolina, Columbia, SC 29028, USA

* Correspondence: Roshan Joseph, Email: rjoseph@email.sc.edu.

ABSTRACT

In this paper, the excitation and propagation of guided waves in multilayer hollow cylinders with piezoelectric wafer active sensor (PWAS) transducers were modeled with the normal mode expansion (NME) method using the semi-analytical finite element (SAFE) formulation. The theoretical development of SAFE for hollow cylindrical structures was introduced and used to obtain guided-wave mode shapes and dispersion curves of multilayer hollow cylinders. The SAFE discretization was applied across the thickness. The layers present in the cylinder were modeled by grouping the elements in the region corresponding to the respective layers. Each finite element region was given the property of the layer that it represented. The number of elements in a layer was determined through convergence studies. The PWAS excitation effect, introduced using the ideal-bonding assumption, was represented by a line-force acting on the PWAS boundary. The SAFE-NME solution obtained in the wavenumber domain was resolved in the physical domain through inverse Fourier transform and residue theorem. Experimental validation of theoretical prediction was performed by comparison with scanning laser Doppler vibrometer (SLDV) measurements from a "6-inch schedule-40" pipe of 11 mm thickness installed with a 7-mm square PWAS transducer for wave excitation. Numerical prediction of the guided wave propagation emanating from the PWAS was first performed and wavefront visualization was obtained. An SLDV area scan of the guided waves generated by the PWAS was then performed and compared with numerical predictions. A good match between experiment and prediction was observed.

KEYWORDS: SAFE; normal mode expansion; hollow cylinders; guided wave propagation

INTRODUCTION

Multi-layer cylindrical structures are used in a wide variety of applications such as nuclear-spent fuel storages, pressure vessels, gas

pipelines, etc. The structural safety of such multi-layer structures needs to be inspected periodically to prevent any catastrophic failure. The aging of the structures may initiate slow structural degradation processes such as corrosion, microcrack formation, material transformations, delamination, etc. leading to complete failure. Guided wave SHM is a solution to detect the structural integrity at the early stage [1]. Understanding the guided wave propagation in multilayer hollow cylindrical structures is a problem of practical interest to use it for nondestructive evaluation (NDE).

Theoretical development of guided wave propagation in hollow cylinders was well studied in the past century. Flexural guided waves in pipes have been understood for decades. Gazis studied the exact-analytical model for guided wave propagation in the hollow cylinder [2]. It was shown that there exists an infinite number of normal modes, including axisymmetric modes and non-axisymmetric modes in an elastic hollow cylinder. Each mode has its characteristics, such as phase velocity, group velocity, etc. Gazis also obtained the general solution of harmonic waves propagating in an infinite long hollow cylinder. Normal mode expansion (NME) of hollow cylinder modes for a force excitation was first studied by Ditri et al. [3]. A closed-form solution for normal mode expansion coefficients for hollow cylinder modes due to a force excitation was derived in this paper. The excitation and propagation of non-axisymmetric longitudinal waves by using NME with different sources are studied by Li et al. [4]. The angular profile due to such excitation is obtained by constructive and destructive interference of amplitude factors of every excited mode. Sun et al. [5] studied flexural torsional wave mechanics and focusing on NME.

Various methods and transducers have been used for selective excitation and propagation of axisymmetric and nonaxisymmetric guided wave modes in hollow cylinders. Many uses comb transducer as well as dry couples normal beam transducer for the generation of axisymmetric guided wave generation in hollow cylinders [6,7]. A transducer array made of a series of normal beam transducers can also be used for axisymmetric guided wave generation [8]. When only a portion of the cylinder might be accessible for source loading, non-axisymmetric guided waves are generated. In such circumstances, the acoustic field is more complicated, and the energy distribution of the wave propagation needs to be known to evaluate the guided wave inspection ability and to perform frequency and angle tuning [3].

Several studies used finite element analysis to study the guided wave propagation in hollow cylindrical structures. Li et al. [9] modeled the guided wave propagation in a pressure vessel using finite element analysis and validated with the experimental investigation. The excitation source was a piezoelectric transducer in their studies. Sause et al. [10] studied the acoustic emission (AE) source modeling and guided wave propagation simulation in metallic as well as composite pressure vessels by using FEA. They have modeled the AE source using buried dipole excitation using the

finite element method to simulate the propagation of AE signals in pressure vessels. The disadvantages of finite element analysis are the requirement of a robust computation facility and the cost of computational time. Many studies were also focused on the improvements in the elements used during finite element discretization to improve the convergence and to reduce the computational time [11,12].

Semi-analytical finite element method (SAFE) has been used for guided wave calculations in hollow cylinders [13]. Long-range calculations can be done with little computational time and memory with the SAFE method since it does not require discretization in the wave propagation direction. Early works of the SAFE method were done by Nelson et al. [14]. They successfully formulated SAFE wave equations for elastic layered orthotropic cylinders and plates through mono-dimensional cross-section interpolation. Afterward, the SAFE method has been effectively used to model guided wave propagation in anisotropic composite cylinders [15], laminated composite plates [16], wedges [17], rails [18], functionally graded cylinders [19], piezoelectric plates [20], laminated piezoelectric cylinders [21], and channel beams [22]. SAFE approach for accounting viscoelastic materials is also developed [23,24].

Another "semi-analytical" approach found in the literature is the one in which a local FEM model is used for wave excitation, whereas a global analytical model is used for wave propagation. Ref. [25] describes such a method in which the PWAS is analyzed as a piezoelectric body affixed to the plate. Under electric excitation, the PWAS generates interaction forces at the junction with the plate; these junction forces excite the guided waves traveling on the plate. An FEM-like discretization using Chebyshev-Lobatto interpolation functions and grid points is successfully used for local analysis. Good simulation of the wavefront generated through a tone-burst excitation is obtained and compared very favorably with experiments. Another semi-analytical local-global approach is described in ref. [26,27] under the name "hybrid-global local" approach. In these references, the local FEM model is used to simulate the wave-damage interaction and to model the scattering of guided waves from the damage; subsequently, the scattered waves are allowed to propagate analytically through the rest of the plate until they reach the sensing locations [26,27].

Even though many studies discussed guided wave excitation and propagation in hollow cylinders using various transducers, the analytical modeling of active structural health monitoring using finite-size PWAS transducers in hollow cylindrical structures was not well explored as in plate-like structures [28–32] to the best knowledge of the authors. The novelty of the present research work is the analytical predictive modeling of finite size piezo transducer for excitation and propagation of guided waves in hollow cylindrical structures. The analytical modeling was performed by using the SAFE approach. The SAFE approach for theoretical modeling of guided wave propagation due to a finite size PWAS excitation in hollow cylinders and experimental validation was not reported

anywhere in the literature. A closed-form expression for finite width PWAS excitation on a multi-layer hollow cylinder was derived using the SAFE approach, which is another important novelty of this research. An ideal bonding condition (also known as the pin-force model) of PWAS to the hollow cylinder was assumed in which all the load transfer is assumed to take place over an infinitesimal region at the PWAS ends [31,32].

In this paper, the theoretical and experimental study of excitation and propagation of guided waves in multilayer hollow cylinders through PWAS transducers by using the SAFE approach is discussed. Normal mode expansion was performed to predict the guided wave propagation in hollow cylinders, and the predicted result was compared with the experimental measurements. This paper is divided into the following sections. Section "**SAFE SOLUTION FOR GUIDED WAVES IN A MULTILAYER HOLLOW CYLINDER**" discusses SAFE theoretical development for guided wave propagation. In Section "**SAFE Dispersion Curves and Modeshapes**" the numerical calculation of dispersion curves for specific multilayer geometry is explained. Section "**Complete Analytical Solution of Guided Wave Propagation**" is on SAFE-NME for guided wave propagation in multilayer hollow cylinders due to a PWAS excitation, and Section "**Simulation of Complete Analytical Solution**" is on numerical prediction based on the theoretical development. Section "**WRAPPED PLATE APPROXIMATION FOR GUIDED WAVE PROPAGATION IN CYLINDERS**" discusses a simplified approach, wrapped plate approximation for guided wave propagation due to ideal bonded PWAS excitation [31] on hollow cylinders and its comparison with the analytical model discussed in Section "**SAFE Dispersion Curves and Modeshapes**". In Section "**EXPERIMENTAL VALIDATION OF ANALYTICAL SOLUTION,**" theoretical predictions are compared with SLDV experimental results. Later a discussion on the convergence of circumferential modes in the analytical formulation is provided. The paper ends with a summary and suggested scope of future work.

SAFE SOLUTION FOR GUIDED WAVES IN A MULTILAYER HOLLOW CYLINDER

This section reviews the SAFE solution methodology for modeling guided wave propagation in hollow cylinders as presented in ref. [1]. For a stress-free hollow cylinder, the governing equation provided by the virtual work principle is given as following.

$$\int_V \delta \mathbf{u}^T \cdot \rho \ddot{\mathbf{u}} dV + \int_V \delta \boldsymbol{\varepsilon}^T \cdot \boldsymbol{\sigma} dV = 0 \tag{1}$$

T is the matrix transpose, ρ is density, $\mathbf{u}$ is the displacement field, σ is the stress field and $\ddot{\mathbf{u}}$ is the second derivative of $\mathbf{u}$ with time t.

The volume integral dV is given $dV = rdrd\theta dz$. For hollow cylinder SAFE, finite element approximation is adopted for r dimension. Exact analytical harmonic solutions are used in θ and z-direction. For harmonic wave

propagation in the *z*-direction, the displacement at any point can thus be represented as follows.

$$\mathbf{u}(r,\theta,z,t) = \sum_{j=1}^{2} \mathbf{N}(r)\mathbf{U}^j e^{i(\xi z + n\theta - \omega t)} \tag{2}$$

Here ξ is the wavenumber in the *z*-direction and *n* represents the circumferential wavenumber. Also, U^j is the nodal displacement vector at the jth element and $N(r)$ is the shape function in the thickness direction *r*. For the two-node element, U^j is a six-element vector and $N(r)$ is a 3 × 6 matrix. Hence the shape function matrix is given as follows:

$$\mathbf{N} = \begin{bmatrix} N_1 & 0 & 0 & N_2 & 0 & 0 \\ 0 & N_1 & 0 & 0 & N_2 & 0 \\ 0 & 0 & N_1 & 0 & 0 & N_2 \end{bmatrix} \tag{3}$$

For two-noded element, using linear shape functions, we get

$$N_1 = \frac{1-k}{2} \tag{4}$$

$$N_2 = \frac{1+k}{2}$$

Here $-1 \le k \le 1$ is the natural coordinate in the *r* direction. The strain displacement relations in cylindrical coordinates are given as follows

$$\varepsilon_{rr} = \frac{\partial u_r}{\partial r} \tag{5}$$

$$\varepsilon_{\theta\theta} = \frac{u_r}{r} + \frac{1}{r}\frac{\partial u_\theta}{\partial \theta}$$

$$\varepsilon_{zz} = \frac{\partial u_z}{\partial z}$$

$$\gamma_{\theta z} = \frac{1}{r}\frac{\partial u_z}{\partial \theta} + \frac{\partial u_\theta}{\partial z}$$

$$\gamma_{rz} = \frac{\partial u_r}{\partial z} + \frac{\partial u_z}{\partial r}$$

$$\gamma_{r\theta} = \frac{1}{r}\frac{\partial u_r}{\partial \theta} + \frac{\partial u_\theta}{\partial r} - \frac{u_\theta}{r}$$

Equations (2) and (4) in (5), will give,

$$\begin{aligned} \boldsymbol{\varepsilon} &= (\mathbf{L}_1 + \mathbf{L}_2)u \\ &= (\mathbf{L}_1 + \mathbf{L}_2)\mathbf{N}(r)\mathbf{U}^j e^{i(\xi z + n\theta - \omega t)} \\ &= (\mathbf{B}_1 + ik\mathbf{B}_2)\mathbf{U}^j e^{i(\xi z + n\theta - \omega t)} \end{aligned} \tag{6}$$

Where

$$\mathbf{L_1} = \begin{bmatrix} \dfrac{\partial}{\partial r} & 0 & 0 \\ \dfrac{1}{r} & \dfrac{1}{r}\dfrac{\partial}{\partial \theta} & 0 \\ 0 & 0 & 0 \\ 0 & 0 & \dfrac{1}{r}\dfrac{\partial}{\partial \theta} \\ 0 & 0 & \dfrac{\partial}{\partial r} \\ \dfrac{1}{r}\dfrac{\partial}{\partial \theta} & \dfrac{\partial}{\partial r}-\dfrac{1}{r} & 0 \end{bmatrix}, \quad \mathbf{L_2} = \begin{bmatrix} 0 & 0 & 0 \\ 0 & 0 & 0 \\ 0 & 0 & \dfrac{\partial}{\partial z} \\ 0 & \dfrac{\partial}{\partial z} & 0 \\ \dfrac{\partial}{\partial z} & 0 & 0 \\ 0 & 0 & 0 \end{bmatrix} \quad (7)$$

$$\mathbf{B_1} = \begin{bmatrix} \dfrac{\partial N_1}{\partial r} & 0 & 0 & \dfrac{\partial N_2}{\partial r} & 0 & 0 \\ \dfrac{N_1}{r} & i\dfrac{n}{r}N_1 & 0 & \dfrac{N_2}{r} & i\dfrac{n}{r}N_2 & 0 \\ 0 & 0 & 0 & 0 & 0 & 0 \\ 0 & 0 & i\dfrac{n}{r}N_1 & 0 & 0 & i\dfrac{n}{r}N_2 \\ 0 & 0 & \dfrac{\partial N_1}{\partial r} & 0 & 0 & \dfrac{\partial N_2}{\partial r} \\ i\dfrac{n}{r}N_1 & \dfrac{\partial N_1}{\partial r}-\dfrac{N_1}{r} & 0 & i\dfrac{n}{r}N_2 & \dfrac{\partial N_2}{\partial r}-\dfrac{N_2}{r} & 0 \end{bmatrix} \quad (8)$$

$$\mathbf{B_2} = \begin{bmatrix} 0 & 0 & 0 & 0 & 0 & 0 \\ 0 & 0 & 0 & 0 & 0 & 0 \\ 0 & 0 & N_1 & 0 & 0 & N_2 \\ 0 & N_1 & 0 & 0 & N_2 & 0 \\ N_1 & 0 & 0 & N_2 & 0 & 0 \\ 0 & 0 & 0 & 0 & 0 & 0 \end{bmatrix} \quad (9)$$

Using the constitutive law the stresses can be computed from the strains by [1]

$$\boldsymbol{\sigma} = \mathbf{C}\boldsymbol{\varepsilon} = \mathbf{C}(\mathbf{B_1} + i\xi\mathbf{B_2})\mathbf{U}^j e^{i(\xi x + n\theta - \omega t)} \quad (10)$$

Here, $\mathbf{C}$ is the stiffness matrix. Substituting Equations (2), (6) and (10) into Equation (1), we get the following equation for an arbitrary element j.

$$(\mathbf{K}_1^j + i\xi\mathbf{K}_2^j + \xi^2\mathbf{K}_3^j - \omega^2\mathbf{M}^j)Q = 0 \quad (11)$$

$$\mathbf{K}_1^j = \iint_{r\ \theta} \mathbf{B}_1^T\mathbf{C}\mathbf{B}_1 r dr d\theta \quad (12)$$

$$\mathbf{K}_2^j = \iint_{r\ \theta} (\mathbf{B}_1^T\mathbf{C}\mathbf{B}_2 - \mathbf{B}_2^T\mathbf{C}\mathbf{B}_1) r dr d\theta \quad (13)$$

$$\mathbf{K}_3^j = \int_r \int_\theta \mathbf{B}_2^T \mathbf{C} \mathbf{B}_2 \, r \, dr \, d\theta \tag{14}$$

$$\mathbf{M}^j = \rho \int_r \int_\theta \mathbf{N}^T \mathbf{N} \, r \, dr \, d\theta \tag{15}$$

Hence Equation (16) can be rewritten as a first-order eigensystem as following

$$\left[\mathbf{A} - \xi\mathbf{B}\right]\begin{bmatrix}\mathbf{U} \\ k\mathbf{U}\end{bmatrix} = 0 \tag{16}$$

where

$$\mathbf{A} = \begin{bmatrix} 0 & \mathbf{K}_1 - \omega^2\mathbf{M} \\ \mathbf{K}_1 - \omega^2\mathbf{M} & \hat{\mathbf{K}}_2 \end{bmatrix}, \mathbf{B} = \begin{bmatrix} \mathbf{K}_1 - \omega^2\mathbf{M} & 0 \\ 0 & -\mathbf{K}_3 \end{bmatrix} \tag{17}$$

For elastic materials, the matrices A and B are $4N \times 4N$. Where N represents the number of elements. The total $4N$ eigenvalues for wave number ξ and eigenvectors for mode shapes can be solved at each frequency from Equation (16). If the original vector U is of dimension M then the dimension of $\begin{bmatrix}\mathbf{U} \\ \xi\mathbf{U}\end{bmatrix}$ is $2M$. At each frequency ω, one obtains $2M$ eigenvalues ξm and corresponding $2M$ left eigenvectors $\hat{\mathbf{V}}_m^L$ ($1 \times 2M$ dimension) and $2M$ right eigenvectors $\hat{\mathbf{V}}_m^R$ ($2M \times 1$ dimension).

SAFE Dispersion Curves and Modeshapes

Dispersion curves

The eigenvalue problem in Equation (16) is solved for the eigenvalues and eigenvectors to get dispersion curves and mode shapes. A scaled-down "TN32 multilayer cylinder" configuration, as shown in Figure 1 was considered for the solution. Tn 32 cylindrical casks are used for the safe storage of nuclear-spent fuel rods. Multiple metallic layers are provided for the structure for the safe storage of the spent fuel rods. For ensuring the safety of the cask and the nuclear-spent fuels, regular non-destructive testing is a convenient methodology. The development of a reliable guided wave structural health monitoring is a good solution for non-destructive testing of multi-layer hollow cylinders similar to TN32 casks. For the analytical investigation of the theoretical formulations derived in the previous sections, a scaled-down TN32 model was considered. The radius and thicknesses of the multilayer cylinder in Figure 1, which are considered for simulation, are presented in Tables 1 and 2. Material properties considered for the layers are given in Table 3. The inner layer was considered of AISI type 304 stainless steel and the outer layer was of AISI 4130 steel.
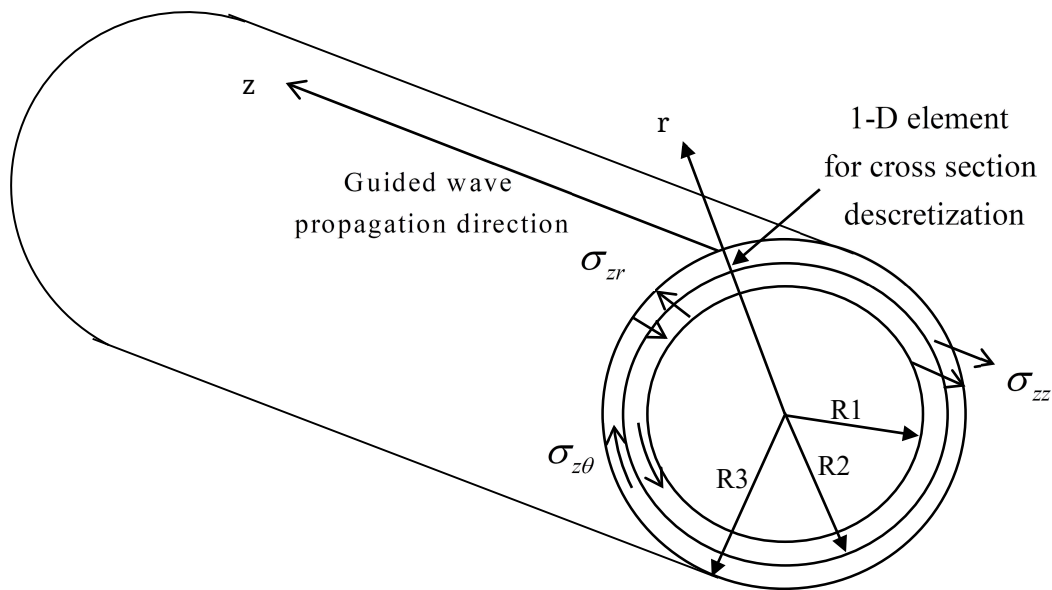
Figure 1. SAFE model for wave propagation in multilayer hollow cylindrical structures.

Table 1. The radius of the multilayer cylinder in Figure 1.

Radius (in mm)	
R1	38
R2	38.5
R3	43.5

Table 2. The thickness of the multilayer cylinder in Figure 1.

Layer thicknesses (in mm)	
T1 (Inner layer)	0.5
T2 (Outer layer	5

Convergence study

The convergence study of the multi-layer cylindrical structure was performed to find out the optimum number of elements required for performing the SAFE analysis. The axisymmetric guided wave modes up to 500 kHz were studied by varying the number of elements (N_e) gradually from 6 to 22. The dispersion curves when N_e was taken as 6, 10, 16, and 22 are presented in Figure 2. As the number of elements increased from 6 to 10, a drastic change in the phase velocity dispersion curve at higher frequency (~500 kHz) was observed. When the number of elements was changed from 10 to 16, and 22 number of elements, very little change in the dispersion curve was observed. Hence 10 number of elements were considered as converged to provide sufficient accuracy.
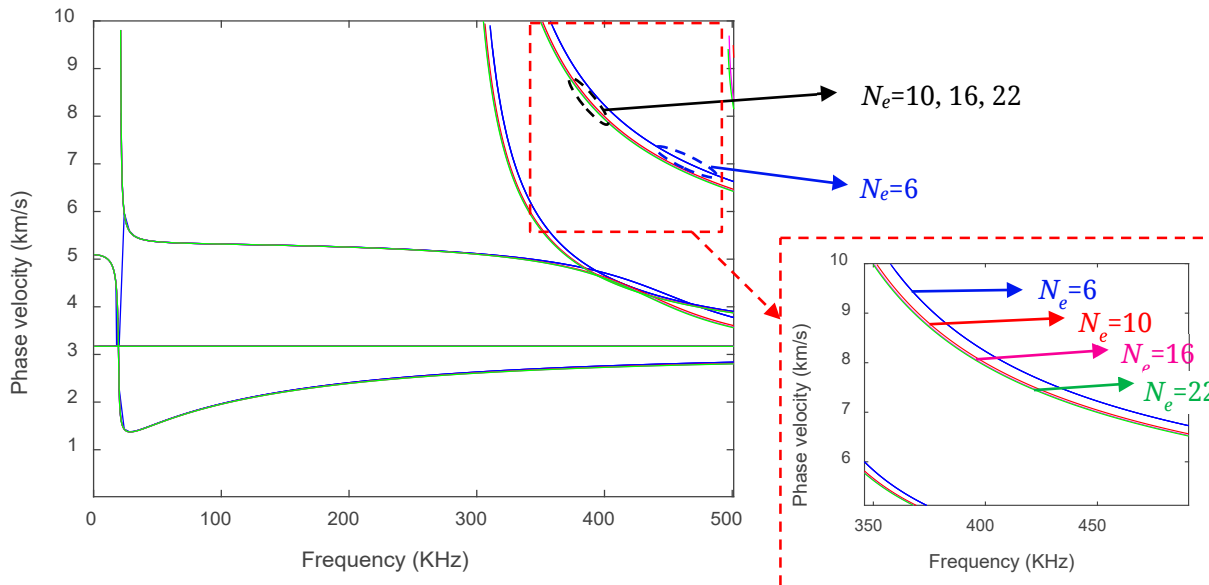
Figure 2. The convergence of the dispersion curve of the multilayer cylinder with the increase in the number of elements (N_e) used for SAFE calculation. The dispersion curves were calculated when the number of elements in the thickness direction was increased from N_e = 6 to 22. The figure represents the overlapped dispersion curves when N_e = 6, 10, 16, 22.

Axisymmetric and non-axisymmetric mode dispersion curves

The guided waves in hollow cylindrical structures can travel in the circumferential and axial direction. For an omnidirectional excitation similar to a PWAS excitation, both circumferential and axial hollow cylinder guided wave modes is generated. In this research, the guided wave propagation in the axial direction in cylindrical structures are discussed.

The axial propagation of guided waves in hollow cylinders consists of longitudinal and torsional modes. The longitudinal wave modes have dominant particle motion in r and z coordinate, whereas torsional wave modes have dominant particle motion in θ coordinates. Generally, the letter "L(m,n)" represents the longitudinal family of modes, and the letter "T(m,n)" represents the torsional family of modes. The letter "m" represents the group order of a mode. The letter "n" represents the circumferential wavenumber. "n = 0" represents the axisymmetric hollow cylinder mode, and "$n \geq 1$" represents a non-axisymmetric hollow cylinder mode.

Given the dimensions and material properties of the multilayer cylinder considered, dispersion curves of the multilayer cylinder are generated by solving Equation (16) and are presented in Figure 3. The dispersion curves are generated for L(1,n), L(2,n), and T(1,n) modes. The circumferential variation of axisymmetric and non-axisymmetric hollow cylinder modes are presented in Figure 4. Axisymmetric modes have zero circumferential nodes. Non-axisymmetric modes have twice the order of axisymmetry circumferential nodes. For example, non-axisymmetric

mode of order one has two circumferential nodes, as we observe from Figure 4. From Figure 3, one can observe that the cutoff frequency of modes in a particular family increases with the circumferential wave number. Therefore, the modes of higher circumferential order appear only at higher frequencies. At higher frequencies, all axisymmetric, as well as non-axisymmetric circumferential modes, converges to Rayleigh wave speed.
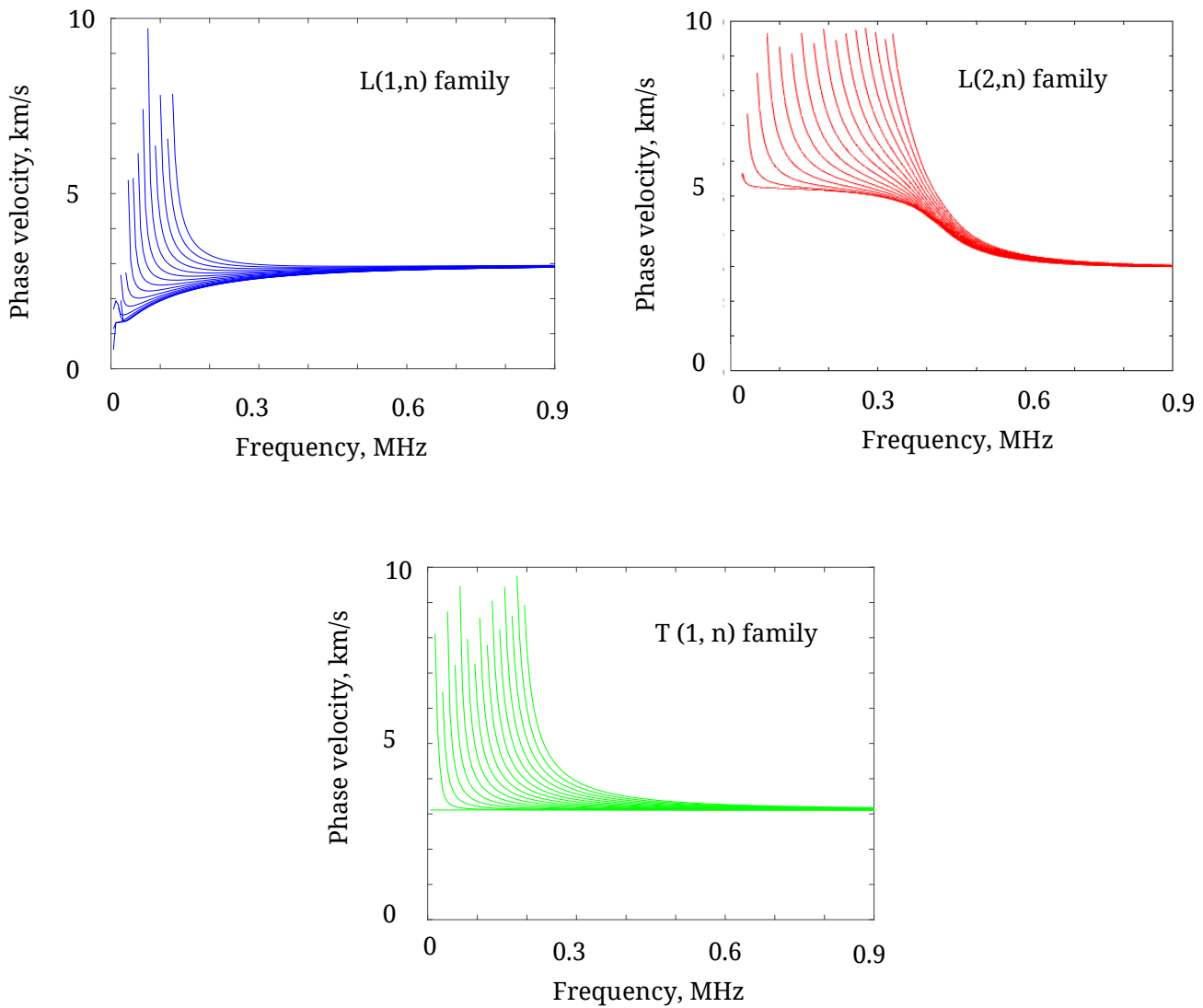

Figure 3. Dispersion curves of the multilayer cylinder generated using the SAFE approach. The dispersion curves are generated for L(1,n), L(2,n) and T(1,n) family.
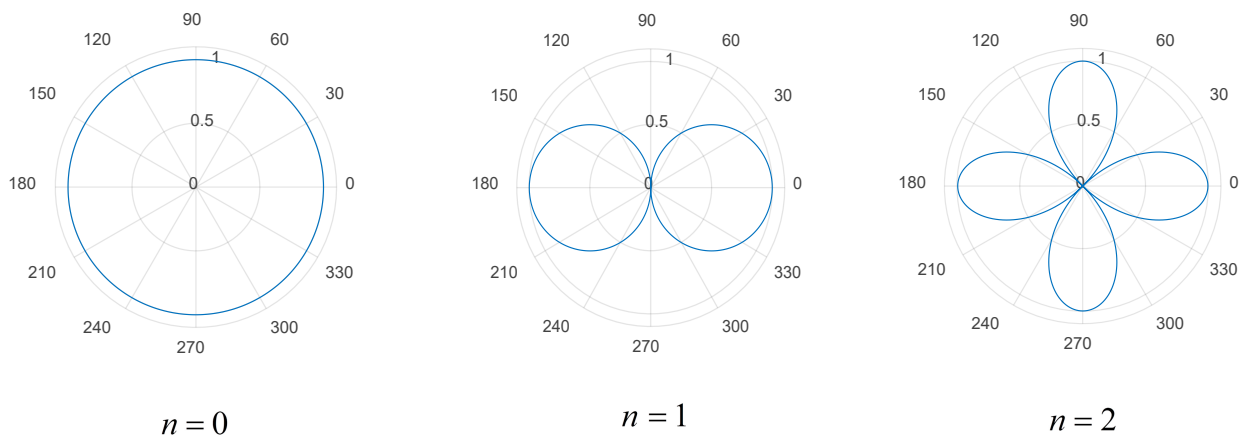
Figure 4. Circumferential variation of axisymmetric and non-axisymmetric hollow cylinder modes with variation in circumferential wave number "n".

Complete Analytical Solution of Guided Wave Propagation

A novel SAFE-NME model for PWAS excitation and propagation of guided waves in a multilayer hollow cylinder is developed in this section. The model discussed in this section considers axisymmetric and non-axisymmetric hollow cylinder guided wave modes. The normal mode expansion (NME) setup of the analytical model for finite-size PWAS excitation on a multilayer hollow cylinder is presented in Figure 5. According to the coordinate system defined, the excitation is non-axisymmetric in nature with respect to angular coordinates; hence, the guided wave propagation also will be non-axisymmetric in nature. So, the non-axisymmetric hollow cylinder guided wave modes is also required to predict the resulting wave motion accurately for a PWAS excitation. Thus, the analytical modeling and numerical calculation of PWAS excitation are complicated. Because many numbers of hollow cylinder modes need to be considered for obtaining the convergence of the solution. Even though the solution can provide an accurate solution, the slow convergence is a disadvantage for a finite size transducer excitation.
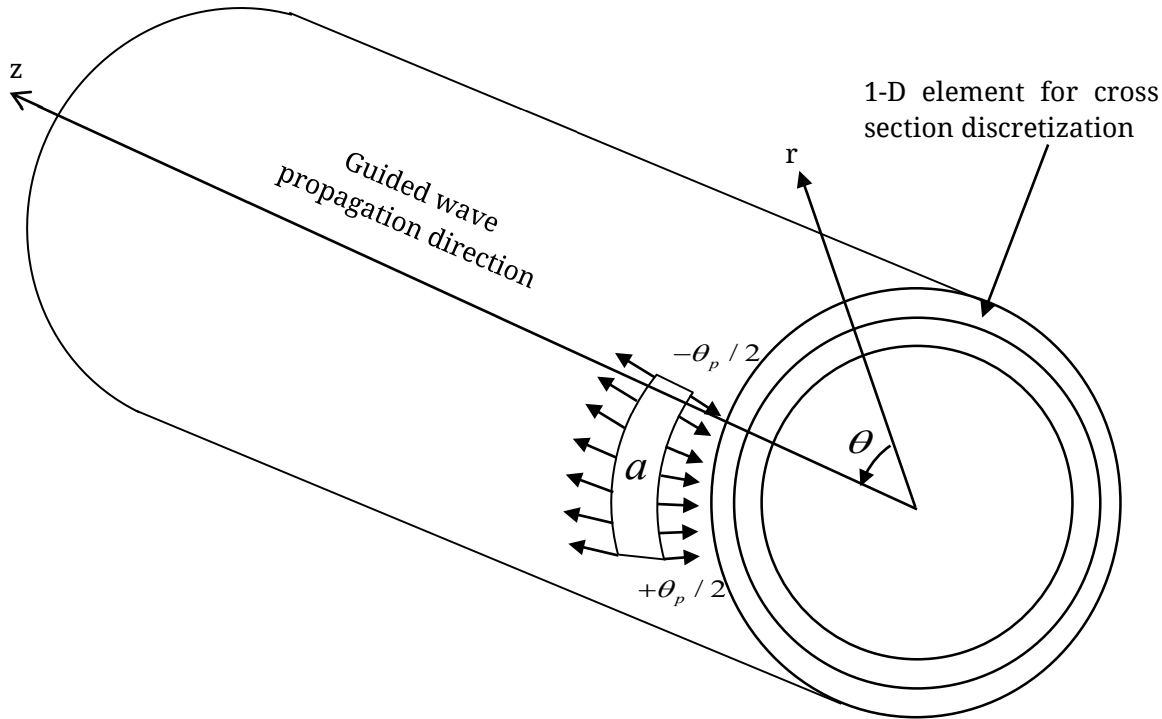
Figure 5. The normal mode expansion (NME) setup of the analytical model for finite-size PWAS excitation on a multilayer hollow cylinder. External traction force acting on the surface of the plate due to PWAS patch excitation is represented as arrows.

The displacement field solution for a non-homogeneous condition where loading $F \neq 0$ can be obtained by using the normal mode expansion method. The displacement field is represented as the summation of the orthogonal hollow cylinder guided wave modes as following [23]

$$\mathbf{U} = \sum_{m,n=1}^{2M} \mathbf{U}_{m,n} \mathbf{\Phi}_{m,n} \tag{18}$$

where, Um,n is the normal mode expansion coefficient of mode m and circumferential order n, given as [33]

$$\mathbf{U}_{m,n} = \frac{\hat{\mathbf{V}}_{m,n}^{L}\mathbf{P}}{(\xi_{m,n}-\xi)\hat{\mathbf{V}}_{m,n}^{L}\mathbf{P}\hat{\mathbf{V}}_{m,n}^{R}}, \quad \xi \neq \xi_{m,n}, m,n = 1,2,...,2M \tag{19}$$

And $\Phi_{m,n}$ is the modeshape vector. Here **P** is the excitation.

To obtain the displacement field in the physical domain from the displacement field in the wavenumber domain in Equation (18), we take inverse Fourier transform with respect to wavenumbers, ξ_z

$$\mathbf{u}(z,\omega) = \frac{1}{2\pi}\int_{-\infty}^{+\infty} \sum_{m,n=1}^{M} \frac{\hat{\mathbf{V}}_{m,n}^{L}\mathbf{P}}{(\xi_{m,n}-\xi)\hat{\mathbf{V}}_{m,n}^{L}\mathbf{P}\hat{\mathbf{V}}_{m,n}^{R}} \mathbf{\Phi}_{m,n} e^{i(\xi_z z)} d\xi_z \tag{20}$$

The excitation due to an ideally bonded PWAS is expressed as the traction acting at the edges of a rectangular PWAS of width, α as represented in Figure 5. The traction acting is non- axisymmetric. The PWAS excitation is considered to act over angular coordinate from $-\theta_p/2$ to $\theta_p/2$ as represented

in the figure. We neglect torsional waves as well as corresponding excitations for the time being since the torsional waves have predominant in-plane tangential displacement.

For a rectangular ideally bonded PWAS excitation [31,32], the forcing functions τ_z are represented as line force as following

$$\tau_z = \tau_0[\delta(r-a)-\delta(r-a)]\prod(\theta/2) \tag{21}$$

Where δ represents the Dirac delta function and $\prod$ represents the rectangular function. Both function together mathematically represents the longitudinal line force excitation given by the PWAS in Figure 5. These line forces are coupled with the relevant surface nodes of the thickness-wise FEM discretization, i.e., with the nodes which are part of the plate surface on which the PWAS is attached. Only some local nodes are affected, i.e., those around the PWAS periphery.

Fourier transform of excitation in Equation (21) is expressed as follows

$$\overline{\tau}_z = -2ia\tau_0 \sin(\xi a)\frac{\sin(n\theta_p/2)}{n} \tag{22}$$

Where, $\dfrac{\sin(n\theta_p/2)}{n\pi}$ is the Fourier transform in polar coordinates of square pulse function from $-\theta_p/2$ to $\theta_p/2$. The integral in Equation (20) could be singular at points corresponding to real roots of hollow cylinder guided wave equation or roots of shear-horizontal (SH) waves or both after substituting $\overline{\tau}_z$. The excitation $\overline{\tau}_z$ will correspond to excitation for propagating longitudinal hollow cylinder guided wave corresponding to the roots. Excitation for longitudinal guided wave propagation due to PWAS, or the component **P** in Equation (20) by considering the line forces are coupled with the relevant surface nodes of the thickness-wise FEM discretization, is written as follows,

$$\mathbf{P} = \begin{bmatrix} \mathbf{0} \\ \hat{\mathbf{F}} \end{bmatrix} \tag{23}$$

where,

$$\hat{\mathbf{F}} = \begin{bmatrix} -2ia\tau_0 \sin(\xi a)\dfrac{\sin(n\theta_p/2)}{n} \\ 0 \\ . \\ . \\ 0 \end{bmatrix} = -2ia\tau_0 \sin(\xi a)\frac{\sin(n\theta_p/2)}{n}\begin{bmatrix} 1 \\ 0 \\ . \\ . \\ 0 \end{bmatrix} \tag{24}$$

$$= -2ia\tau_0 \sin(\xi a)\frac{\sin(n\theta_p/2)}{n}\hat{\mathbf{F}}_1$$

Hence, we write,

$$\mathbf{P} = \mathbf{P_1}\left(-2ia\tau_0 \sin(\xi a)\frac{\sin(n\theta_p / 2)}{n}\right) = \mathbf{P_1}\left(-2ia\tau_0 \sin(\xi a)\frac{\sin(n\theta_p / 2)}{n}\right) \quad (25)$$

where,

$$\mathbf{P_1} = \begin{bmatrix} \mathbf{0} \\ \hat{\mathbf{F}}_\mathbf{1} \end{bmatrix} \quad (26)$$

Substituting Equation (26) into Equation (20) we get,

$$\mathbf{u}(z,\omega) = \frac{1}{2\pi}\int_{-\infty}^{+\infty}\sum_{m,n=1}^{M}\frac{\hat{\mathbf{V}}_{m,n}^{L}\mathbf{P_1}}{(\xi_{m,n} - \xi)\hat{\mathbf{V}}_{m,n}^{L}\mathbf{P}\hat{\mathbf{V}}_{m,n}^{R}}\mathbf{\Phi}_{m,n}\left(-2ia\tau_0 \sin(\xi a)\frac{\sin(n\theta_p / 2)}{n}\right)e^{i(\xi_z z)}d\xi_z \quad (27)$$

Applying residue theorem for integrating Equation (27), we get the expression for displacement field as following

$$\mathbf{u}(z,\omega) = \frac{1}{\pi}\sum_{m,n=1}^{M}(-ia\tau_0 \sin(\xi_{m,n}a))\frac{\hat{\mathbf{V}}_{m,n}^{L}\mathbf{P_1}}{\hat{\mathbf{V}}_{m,n}^{L}\mathbf{P}\hat{\mathbf{V}}_{m,n}^{R}}\mathbf{\Phi}_{m,n}\frac{\sin(n\theta_p / 2)}{n}e^{i(\xi_{m,n}z)} \quad (28)$$

Simulation of Complete Analytical Solution

The analytical solution derived in Equation (28) is used for simulation of guided wave propagation due to a PWAS excitation in the scaled-down TN32 multilayer hollow cylinder discussed in Section "**Dispersion curves**". The simulation method used is presented in the flow chart in Figure 6. First, the Fourier transform of the excitation signal, $\mathbf{P_1}$, was performed. Then, the structural transfer function $G(z,\omega)$ was calculated by using Equation (28). Then, the excitation signal was multiplied with the structural transfer function in the frequency domain to obtain the frequency domain of the signal at the sensing location. Finally, the inverse Fourier transform of the multiplication result was performed to obtain the time domain signal.

For numerical simulation, 60 kHz Hanning windowed 3-count tone burst excitation is assumed to be applied in the longitudinal direction by using a PWAS. A longitudinal excitation excites only longitudinal modes and torsional modes. The relative amplitude factors for L(1,n) and L(2,n) families for different circumferential orders, n, are plotted by using the structural transfer function equation $G(z,\omega)$ discussed in Figure 6 and are presented in Figure 7. Coefficients are obtained for axisymmetric circumferential order mode (n = 0) and first 64 non-axisymmetric circumferential order modes ($0 < n \leq 64$). The axisymmetric mode has the highest amplitude. With variation in the order of non-axisymmetry, the change in the amplitude factor can be clearly understood from the figure for the specific dimension of the PWAS. The number of modes needs to be considered for the prediction of the accurate solution depends on the amplitude factor and the excitation frequency. Figure 8a represents the frequency spectrum of the 60-kHz 3-count tone burst. The limit of the

major frequency content of the excitation signal is marked in green lines. The phase velocity dispersion curves of L(1,n) and L(2,n) mode superimposed with the excitation frequency limit is presented in Figure 8b,c. One can neglect the modes, which have cutoff frequency outside the excitation frequency limits without losing considerable accuracy to the prediction, because of their negligible contribution in the final solution. Hence from Figure 8, we can conclude that for L(1,n) family, first 16 circumferential order modes, and for L(2,n) family, the first seven circumferential order modes need to be considered for the predictive modeling for the present excitation frequency. The numerical prediction in this section was performed accordingly.

Out of plane displacement waveform was predicted for L(1,n) and L(2,n) family of modes and are presented in Figure 9. Only L(1,n) and L(2,n) family of modes are considered for the simulation since the torsional modes have predominant radial displacements. L(2,n) family of mode has higher wave speed compared to L(1,n) mode. Hence, they arrive earlier than L(1,n) mode. After the arrival of L(2,n) and L(1,n) mode, wrapping around of the longitudinal modes occur, which can also be observed from the plot. The amplitude of L(2,n) mode is very less compared to L(1,n) mode at the present frequency.
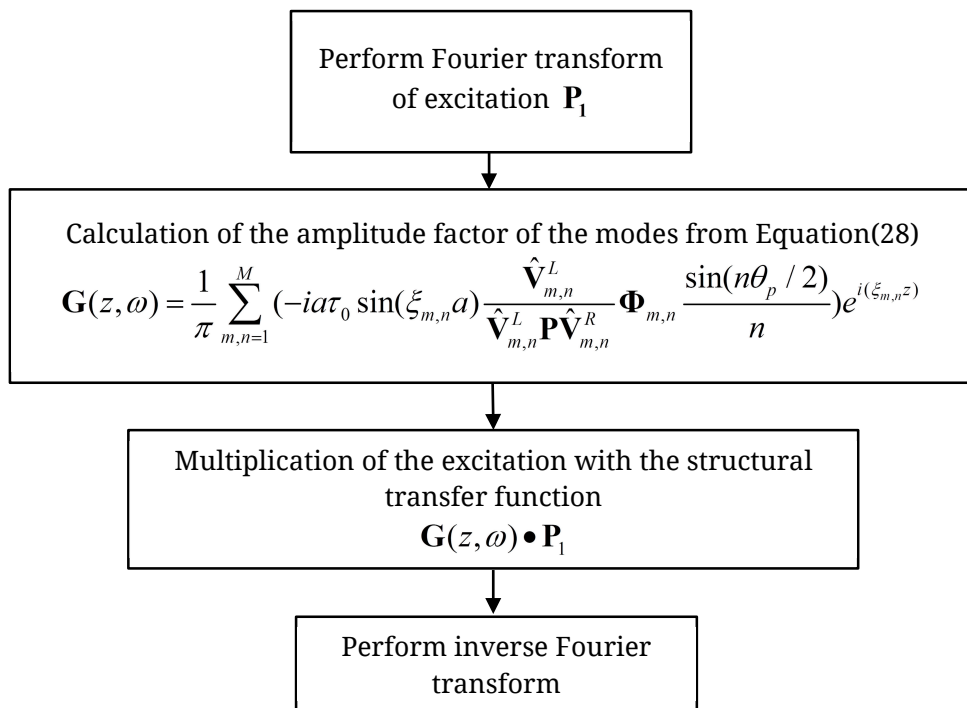
Perform Fourier transform of excitation $\mathbf{P}_1$

Calculation of the amplitude factor of the modes from Equation(28)

$$\mathbf{G}(z,\omega) = \frac{1}{\pi} \sum_{m,n=1}^{M} (-ia\tau_0 \sin(\xi_{m,n}a) \frac{\hat{\mathbf{V}}_{m,n}^{L}}{\hat{\mathbf{V}}_{m,n}^{L}\mathbf{P}\hat{\mathbf{V}}_{m,n}^{R}} \mathbf{\Phi}_{m,n} \frac{\sin(n\theta_p/2)}{n}) e^{i(\xi_{m,n}z)}$$

Multiplication of the excitation with the structural transfer function

$$\mathbf{G}(z,\omega) \bullet \mathbf{P}_1$$

Perform inverse Fourier transform

Figure 6. The flow chart of the simulation method used for predictive modeling of guided wave propagation in a hollow cylinder.
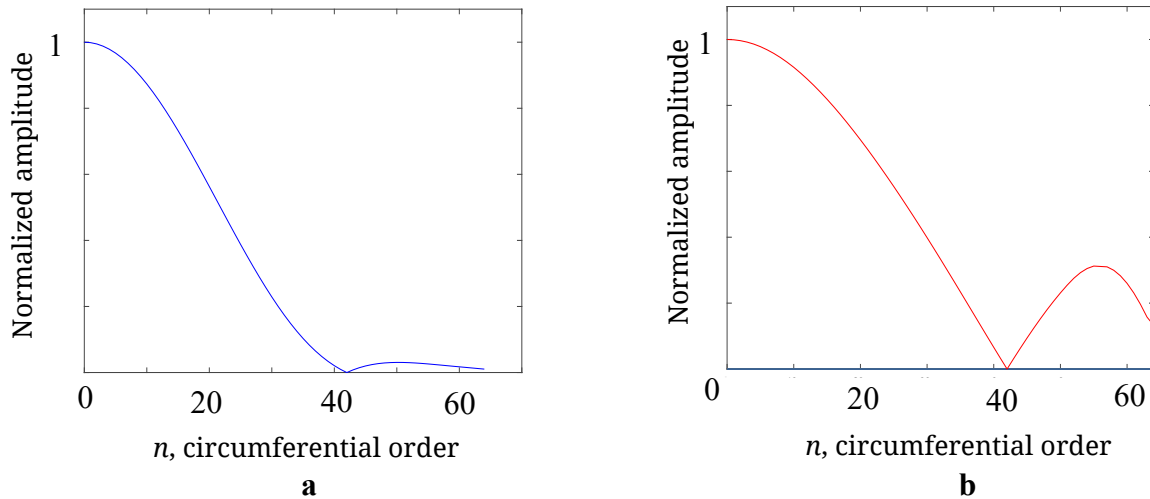
Figure 7. Relative amplitude factors of axisymmetric (circumferential order n = 0) and non-axisymmetric (circumferential order n > 0) wave modes (**a**) For L(1,n) family of modes and (**b**) For L(2,n) family of modes.
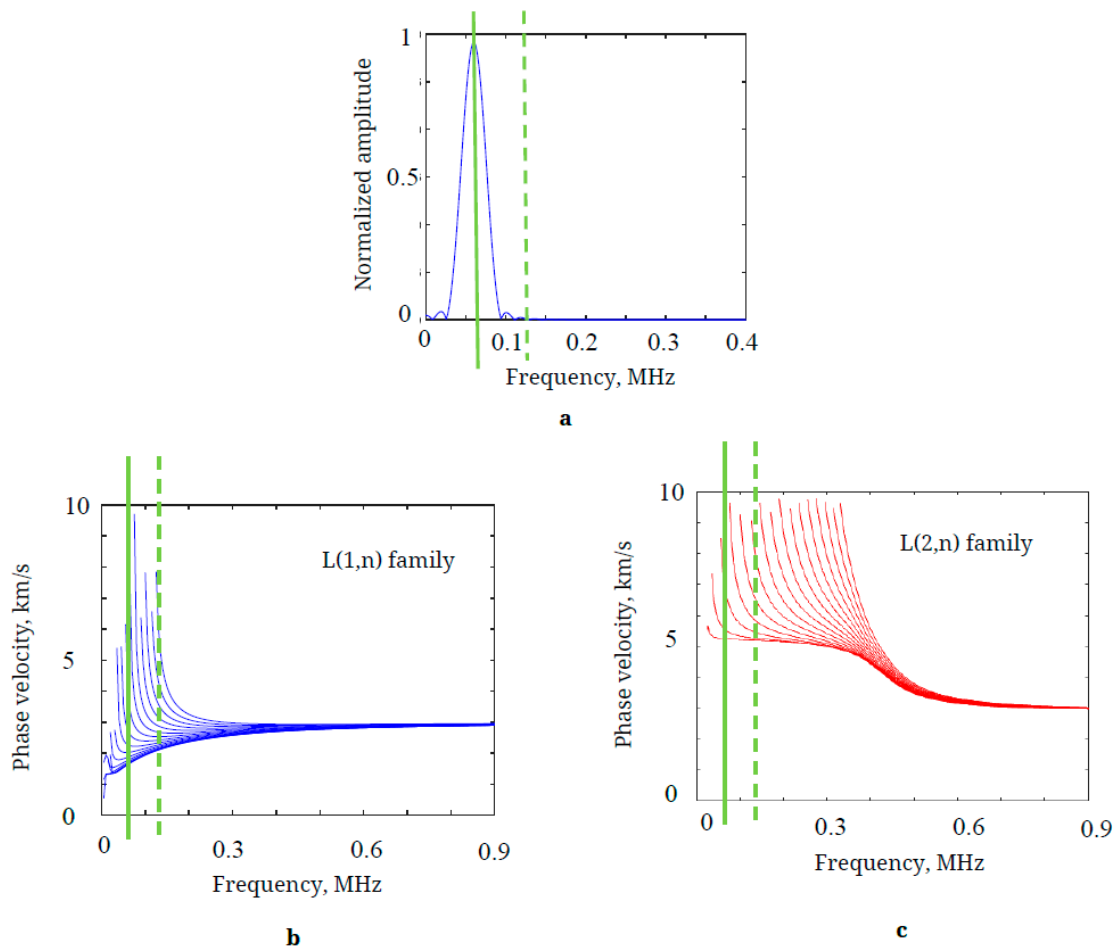

Figure 8. The selection of the number of circumferential order to be considered for normal mode expansion. (**a**) 60 kHz 3-count tone burst frequency spectrum. The excitation frequency major frequency content limits are marked by green lines. (**b**) L(1,n) family of mode and excitation frequency limit. (**c**) L(2,n) family of mode and the excitation frequency limit. The contribution of modes having a cut-off frequency outside the frequency limit is negligible in the normal mode expansion.
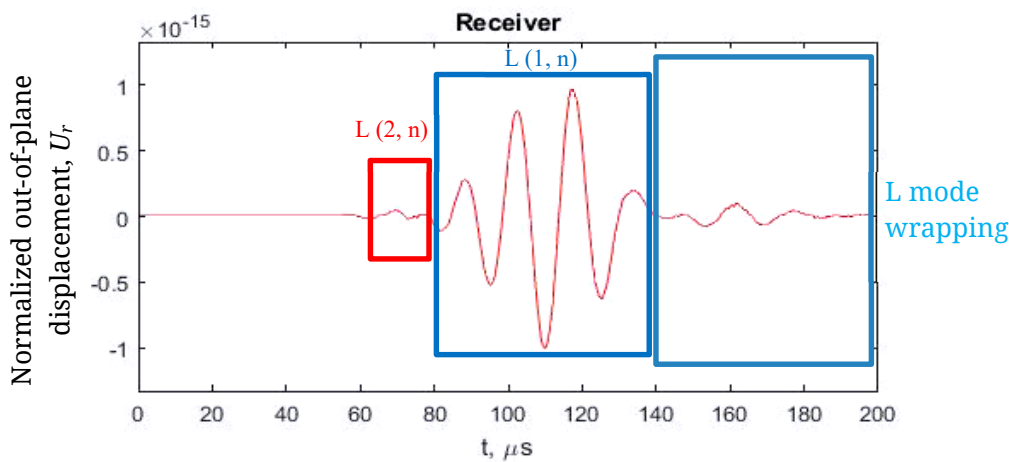
Figure 9. Normalized out of plane displacement at a distance of 170 mm and 0-degree circumferential variation from the PWAS excitation location.

WRAPPED PLATE APPROXIMATION FOR GUIDED WAVE PROPAGATION IN CYLINDERS

In the previous section, the complete solution of guided propagation in multilayered hollow cylinders due to a finite size PWAS was analyzed. A multilayered hollow cylinder can be assumed to be a plate which is wrapped around to form the geometry like in Figure 10. If the cylinder is assumed as a wrapped plate, the guided wave propagation in the hollow cylinder can be considered as plate guided waves propagating in a curved geometry whose edges are finely welded together. This simplified approach is used for modeling guided wave propagation for the present hollow cylinder geometry. The simplified approach has many advantages and disadvantages compared to the complete solution. First, the simplified approach is very easy to understand, model and visualize, because the plate guided wave equations are very simple and well developed for metallic as well as composite structures. The complete solution of finite size PWAS excitation on the hollow cylinder is more precise, but it involved guided wave families that are not so familiar to every engineer. The simplified approach is an approximation, but it used Lamb waves and SH waves, which are more familiar to many engineers. Our study shows that the two concepts are equivalent to the low-order modes; it also builds a bridge of understanding between the complicated cylinder guided waves and the simpler plate guided waves. Second, many researchers have explored the theory of guided wave propagation in various plate structures very well [25–27]. The simplified approach concept allows utilizing these theoretical developments to hollow cylinders. One disadvantage of the simplified approach is the dependence of the convergence of the simplified approach to the complete solution on the curvature of the cylindrical structure. The solution may not be accurate for high curvature structures.
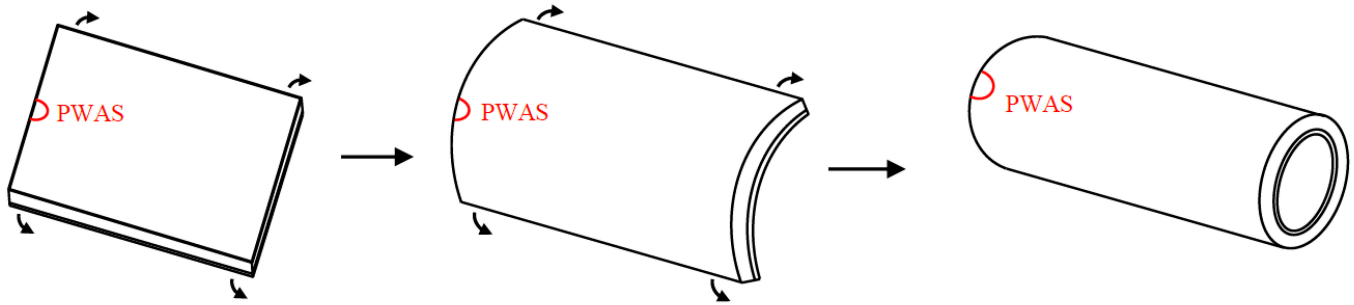
Figure 10. Wrapping a multilayer plate to form a cylinder. This concept is used for modeling Guided wave propagation is in multilayer cylinder This concept considers plate guided wave modes numerically manipulated to predict cylinder guided wave modes due to a PWAS excitation.

For a PWAS bonded to a cylinder, wrapped plate approximation of guided wave propagation was assumed and the simulation was performed. For guided wave propagation in a multilayer plate, the modeling was performed by using the SAFE approach [1].

SAFE adopts harmonic domain formulation $e^{i(\xi x - \omega t)}$, to describe the wave behavior in the wave propagation direction x with ξ representing the wavenumber, ω the angular frequency, and t is the time. The finite element discretization of the SAFE method takes place in the thickness direction of the waveguide (Figure 11). A governing equation for the wave motion of each element can be obtained through the virtual work principle, as represented in Equation (1).

$$\int_V \delta\mathbf{u}^T \cdot \rho\ddot{\mathbf{u}} dV + \int_V \delta\mathbf{\varepsilon}^T \cdot \mathbf{\sigma} dV = 0 \tag{29}$$

For a one-dimensional discretization and adopting the conventional finite element assembly methodology, we obtain the eigenvalue problem in the global coordinate system as follows [1]:

$$(\mathbf{K}_1 + \xi\hat{\mathbf{K}}_2 + \xi^2\mathbf{K}_3 - \omega^2\mathbf{M})\mathbf{Q} = 0 \tag{30}$$

Equation (30) can be rewritten as a first-order eigensystem as follows:

$$\left[\mathbf{A} - \xi\mathbf{B}\right]\begin{bmatrix}\hat{\mathbf{Q}} \\ k\hat{\mathbf{Q}}\end{bmatrix} = 0 \tag{31}$$

with

$$\mathbf{A} = \begin{bmatrix} 0 & \mathbf{K}_1 - \omega^2\mathbf{M} \\ \mathbf{K}_1 - \omega^2\mathbf{M} & \hat{\mathbf{K}}_2 \end{bmatrix}, \mathbf{B} = \begin{bmatrix} \mathbf{K}_1 - \omega^2\mathbf{M} & 0 \\ 0 & -\mathbf{K}_3 \end{bmatrix} \tag{32}$$

If the original vector $\hat{\mathbf{Q}}$ is of dimension M, then the dimensions of $\begin{bmatrix}\hat{\mathbf{Q}} \\ \xi\hat{\mathbf{Q}}\end{bmatrix}$, $\mathbf{A}$ and $\mathbf{B}$ are 2M. At each frequency ω, one obtains 2M. Eigenvalues ξ_m and corresponding 2M left eigenvectors $\hat{\mathbf{V}}_m^L$ ($1 \times 2M$ dimension) and 2M right eigenvectors $\hat{\mathbf{V}}_m^R$ ($2M \times 1$ dimension).
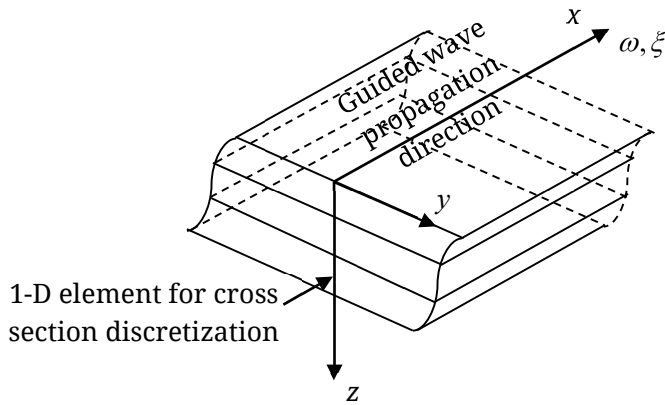
Figure 11. SAFE model for wave propagation in plate structures.

PWAS Excitation Using NME in a Multilayer Plate

The displacement field solution for a non-homogeneous condition where loading F ≠ 0 can be obtained by using the normal mode expansion method. The displacement field will be the summation of the orthogonal modes as following [23,34]

$$\mathbf{U} = \sum_{m=1}^{2M} \mathbf{U}_m \boldsymbol{\Phi}_m \tag{33}$$

Where Φ_m is the mode shape vector and U_m is the normal mode expansion coefficient given as [33]

$$\mathbf{U}_m = \frac{\hat{\mathbf{V}}_m^L \mathbf{P}}{(\xi_m - \xi)\hat{\mathbf{V}}_m^L \mathbf{P} \hat{\mathbf{V}}_m^R}, \quad \xi \neq \xi_m, m = 1, 2, ..., 2M \tag{34}$$

For obtaining the displacement field in the physical domain from the displacement field in the wavenumber domain in Equation (33), we take inverse Fourier transform with respect to wavenumbers, ξ_x, ξ_y, i.e.,

$$\mathbf{u}(x, y, \omega) = \frac{1}{4\pi^2} \int_{-\infty}^{+\infty} \int_{-\infty}^{+\infty} \sum_{m=1}^{M} \frac{\hat{\mathbf{V}}_m^L \mathbf{P}}{(\xi_m - \xi)\hat{\mathbf{V}}_m^L \mathbf{P} \hat{\mathbf{V}}_m^R} \boldsymbol{\Phi}_m e^{i(\xi_x x + \xi_y y)} d\xi_x d\xi_y \tag{35}$$

Following ref. [34], one can derive the closed-form expression for a PWAS excitation presented in Figure 12 in a multilayer cylinder as following,

$$\mathbf{u}(r, \omega) = \frac{ia\tau_0}{4} \sum_{m=1}^{M} (J_1(\xi_m a)) \frac{\hat{\mathbf{V}}_m^L \mathbf{P}_1}{\hat{\mathbf{V}}_m^L \mathbf{P} \hat{\mathbf{V}}_m^R} \boldsymbol{\Phi}_m \xi_m \left(\sqrt{\frac{1}{\pi \xi_m r}} e^{i\xi_m r} \right) \tag{36}$$

Here, excitation for Lamb wave propagation due to PWAS, or the component P in Equation (36) is written as

$$\mathbf{P} = \begin{bmatrix} \mathbf{0} \\ \hat{\mathbf{F}} \end{bmatrix} \tag{37}$$

where,

$$\hat{\mathbf{F}} = \begin{bmatrix} -ia\tau_0 J_1(\xi a)\cos\theta \\ 0 \\ . \\ . \\ 0 \end{bmatrix} = \begin{bmatrix} 1 \\ 0 \\ . \\ . \\ 0 \end{bmatrix} (-ia\tau_0 J_1(\xi a)\cos\theta) = \hat{\mathbf{F}}_1 (-ia\tau_0 J_1(\xi a)\cos\theta) \tag{38}$$

Hence, we write,

$$\mathbf{P} = \mathbf{P}_1(-ia\tau_0 J_1(\xi a)\cos\theta) = \mathbf{P}_1(-ia\tau_0 J_1(\xi a)\xi_x/\xi) \tag{39}$$

where,

$$\mathbf{P}_1 = \begin{bmatrix} \mathbf{0} \\ \hat{\mathbf{F}}_1 \end{bmatrix} \tag{40}$$
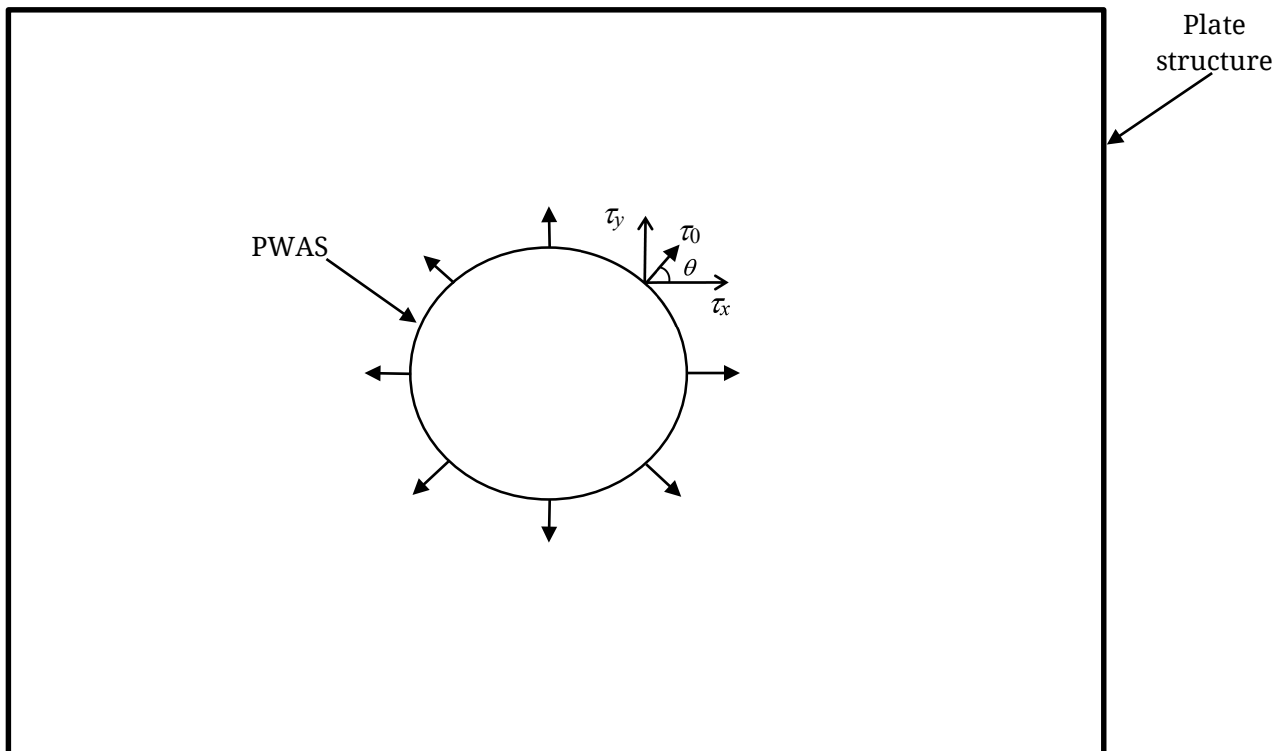
Figure 12. Traction acting on the surface of the plate due to PWAS excitation.

Simulation of Wrapped Plate Guided Wave Propagation

The phase velocity dispersion curve of a 5.5 mm multilayered plate with layer dimensions and material properties as given in Tables 2 and 3 is obtained by solving Equation (31) numerically. Six quadratic elements were considered for calculating dispersion curve and mode shapes from SAFE. The phase velocity dispersion curve obtained from SAFE is presented in Figure 13a and the group velocity dispersion curve is presented in Figure 13b.

Table 3. Material properties of layers in the multilayer cylinder.

Material	Modulus of elasticity (GPa)	Poisson's ratio	Density (kg/m³)
AISI type 304 stainless steel (Inner layer)	193	0.29	8000
AISI 4130 steel (Outer layer)	205	0.29	7850
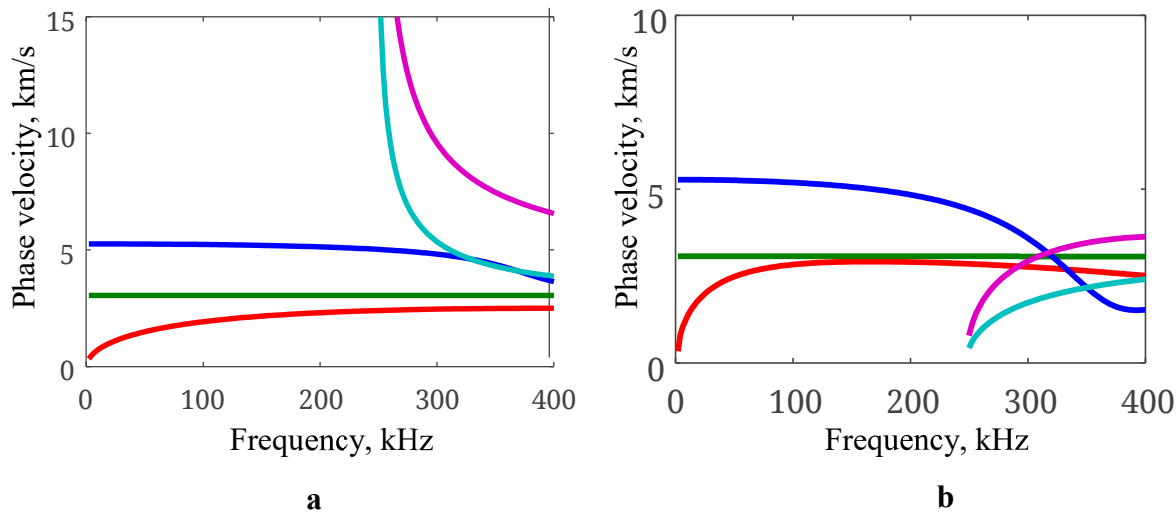
Figure 13. (**a**) Phase velocity dispersion curve of 0.5–5 mm multilayered steel plate (**b**) Group velocity dispersion curve.

For simplifying the simulation method, a wrapped plate assumption was adopted for the multi-layered cylinder. Simulation of plate guided wave propagation was performed by using Equation (36) for a PWAS excitation. The excitation was assumed to be at 60 kHz. 3D wave propagation simulation figure as well as out of plane displacement at sensor location (160 mm *z* distance and 0-degree angular distance) was plotted and is presented in Figure 14. Because of the higher wave speed of S0 mode, the S0 mode arrives earlier compared to A0 mode. For the out of plane displacement, the S0 mode has a relatively very low amplitude compared to A0 mode. After the arrival of S0 and A0 mode, the guided wave, which is wrapping around the hollow cylinder, reaches the sensing location as a third wave packet. The wrapped guided wave mode is equivalent to the hollow cylinder circumferential Lamb type (CLT) waves.
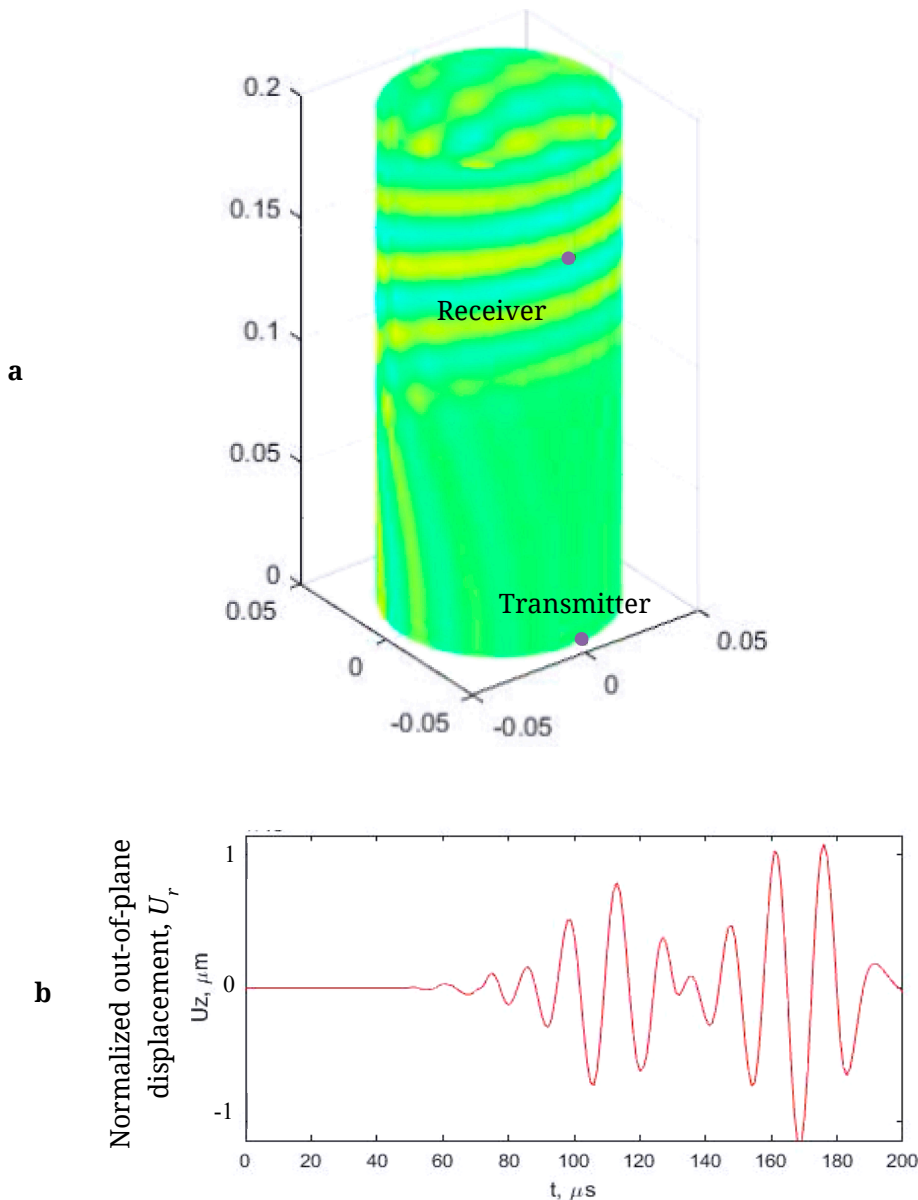
Figure 14. Wrapped plate approximation simulation of the multilayered cylinder for 60 kHz 3.5 count tone burst excitation (**a**) 3d guided wave propagation; (**b**) out-of-plane displacement at a z location of 160 mm and angular location of 0 degrees from the transmitter.

Comparison of the Complete Analytical Model and Wrapped Plate Model

A comparison of the complete analytical model and wrapped plate approximation model was performed by comparing the out of plane velocity at 160 mm *z* distance and 0-degree angular distance from the excitation source. The predictions are presented in Figure 15.
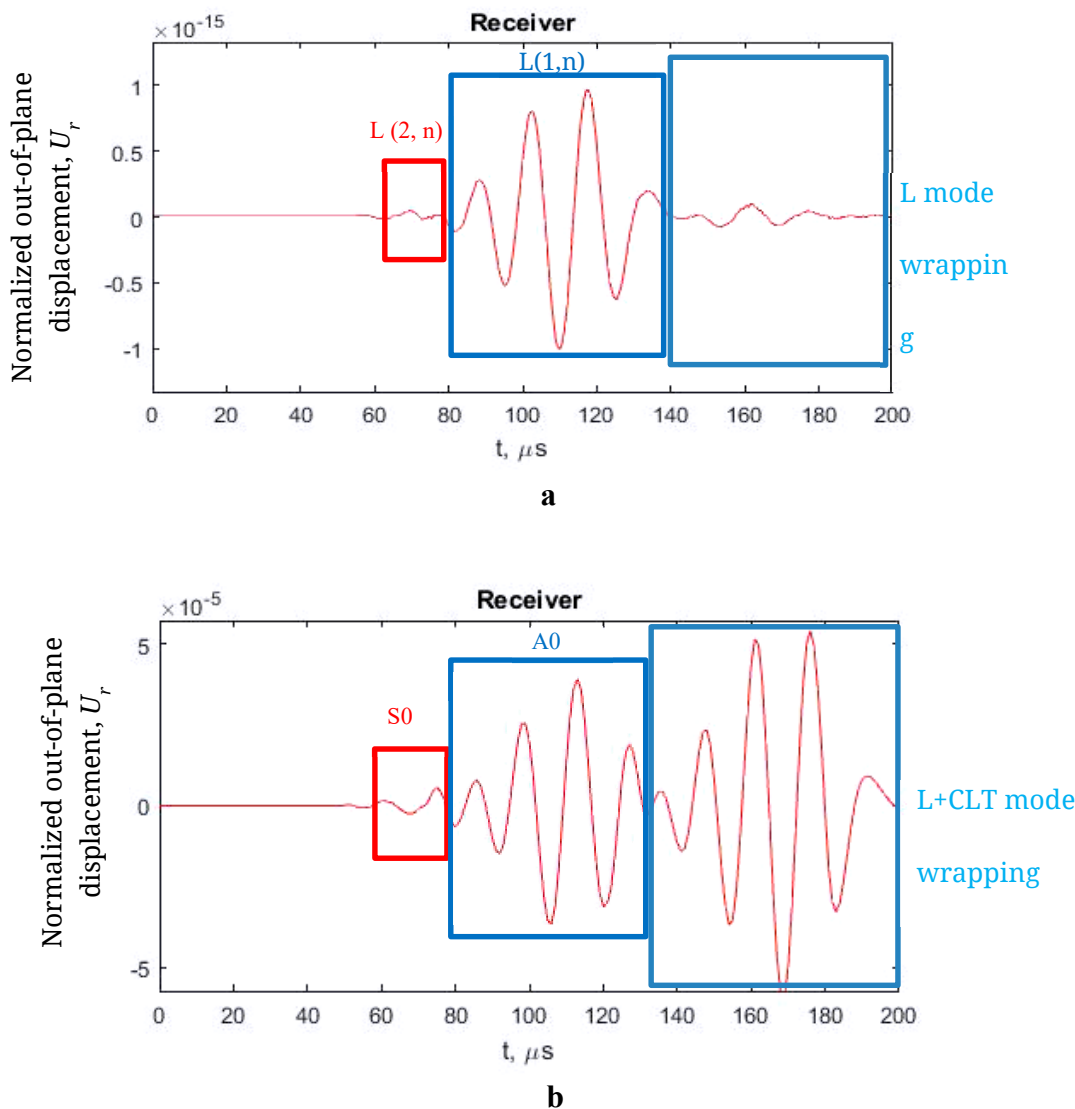
Figure 15. Comparison of the complete analytical model and wrapped plate approximation prediction (**a**) Complete analytical model (**b**) Wrapped plate approximation model.

The L(2,n) family of modes in the complete analytical model corresponds to S0 mode in a wrapped plate approximation model, whereas L(1,n) mode in the complete analytical model corresponds to A0-mode in the wrapped plate approximation model. The complete analytical model considers only longitudinal, guided waves. Wrapping around the hollow cylinder of the longitudinal modes are visible after the arrival of L(1,n) mode in the analytical model. Due to circumferential excitation of PWAS, circumferential Lamb type waves are generated. Wrapped plate approximation model considers the circumferential Lamb type waves by default; hence, we observe a higher amplitude third wave packet after the arrival of A0 mode. On the other hand, the circumferential Lamb type wave packet is missing in the complete analytical model, because the present solution considers only longitudinal hollow cylinder guided wave modes.

EXPERIMENTAL VALIDATION OF ANALYTICAL SOLUTION

Experimental validation of theoretical developments was performed on a "6-inch schedule 40" pipe. The pipe was made of T304 steel material (Modulus of elasticity: 193 GPa, Poisson's ratio: 0.29, Density: 8000 kg/m^3). The inner radius of the pipe was 77.9 mm and the wall thickness of the pipe was 11 mm. A Hanning windowed 3-count tone burst at 90 kHz central frequency excitation was applied using a square PWAS (APC 850: 7 mm × 7 mm dimension and 0.2 mm thickness). The instrumentation used and experimental set up for measurement is provided in Figure 16a, and Figure 16b. A 14-volt peak to peak 90 kHz 3 count tone burst excitation was generated using an Agilent 33120A function generator. The signal generated was amplified to 140 V peak to peak using an HSA 4014 power amplifier. The out of plane velocity component of ultrasonic guided wave propagation is sensed by OFV-505 laser head and processed by scanning laser Doppler vibrometer (SLDV) system. The measurement of the out of plane velocity was conducted through SLDV scans in different directions and the measurement was post-processed. Thus, the hybrid PWAS-SLDV system was used for the measurements. Under the electrical excitation, the PWAS undergo expansion and contraction and generates guided waves in the hollow cylinder. The generated guided waves travel by out-spreading in the area of the hollow cylinder and undergo geometric spreading, causing exponential decrement in the amplitude, undergo dispersion and are received by the SLDV finally.

In order to validate the simulation, the proposed SAFE approach in Section "**Complete Analytical Solution of Guided Wave Propagation**" was used to perform the simulation of the time response of guided wave propagation in a "6-inch schedule 40" pipe. The SAFE method was used to obtain the dispersion curves and mode shapes of the pipe using the material properties and geometry. Then the SAFE approach was used for predictive modeling of guided wave propagation in the pipe and compared with the experimental observation. A very good match of experiment and simulation was observed.

The Equation (16) was solved numerically for the dimensions and material properties of the pipe to obtain the dispersion curves. The dispersion curves of L(1,n) and L(2,n) family of modes are presented in Figure 17. It can be noted that the dispersive nature of L(1,n) and L(2,n) family of modes change depending on the circumferential order, 'n' of the mode. L(2,1) is not very dispersive at the frequency below 250 kHz. But, as the circumferential order increases, the modes in L(2,n) family becomes highly dispersive. Variations in the dispersive nature of L(1,n)-mode was also observed with increment in the circumferential order. Theoretical prediction of the elastic wave propagation was obtained by using the Equation (28). A comparison of experimental measurements with theoretical predictions is presented in Figure 18. Figure 18a represents the theoretical prediction of the wave propagation animation plot at an instant, and Figure 18b represents the waveform at 150 mm distance from PWAS. Figure 18c and Figure 18d represent the corresponding

experimental predictions. The theoretical predictions match very closely with the experimental measurements, as we observe from Figure 18c and Figure 18d. L(2,n) family of mode travel at a higher speed compared to L(1,n) mode. The out of plane component of L(2,n) mode is very low compared to L(1,n) mode at the present frequency (90 kHz), which can be observed in theoretical prediction as well as in the experiment.
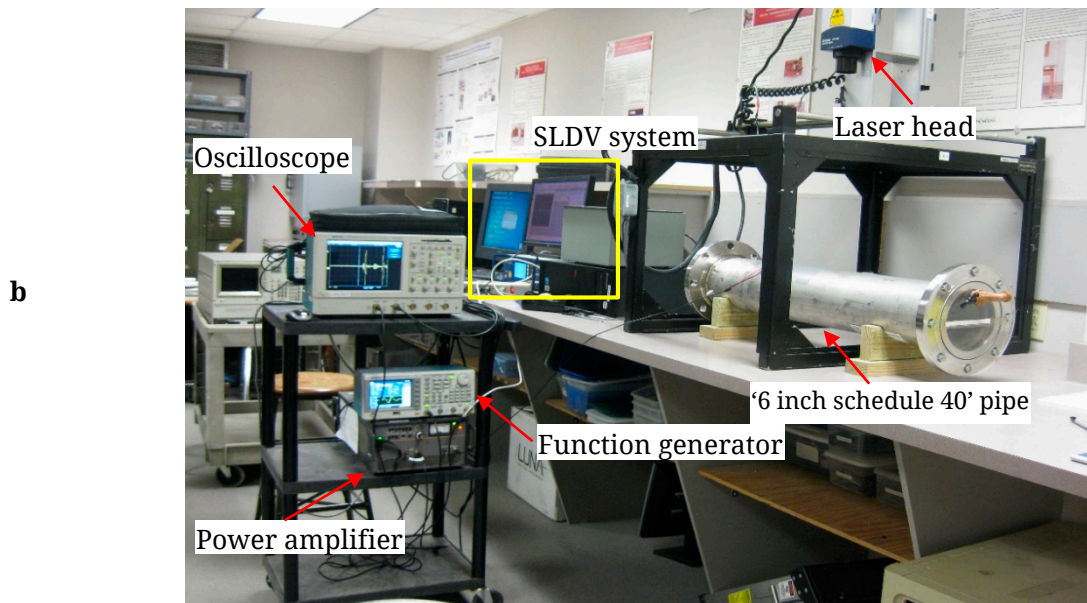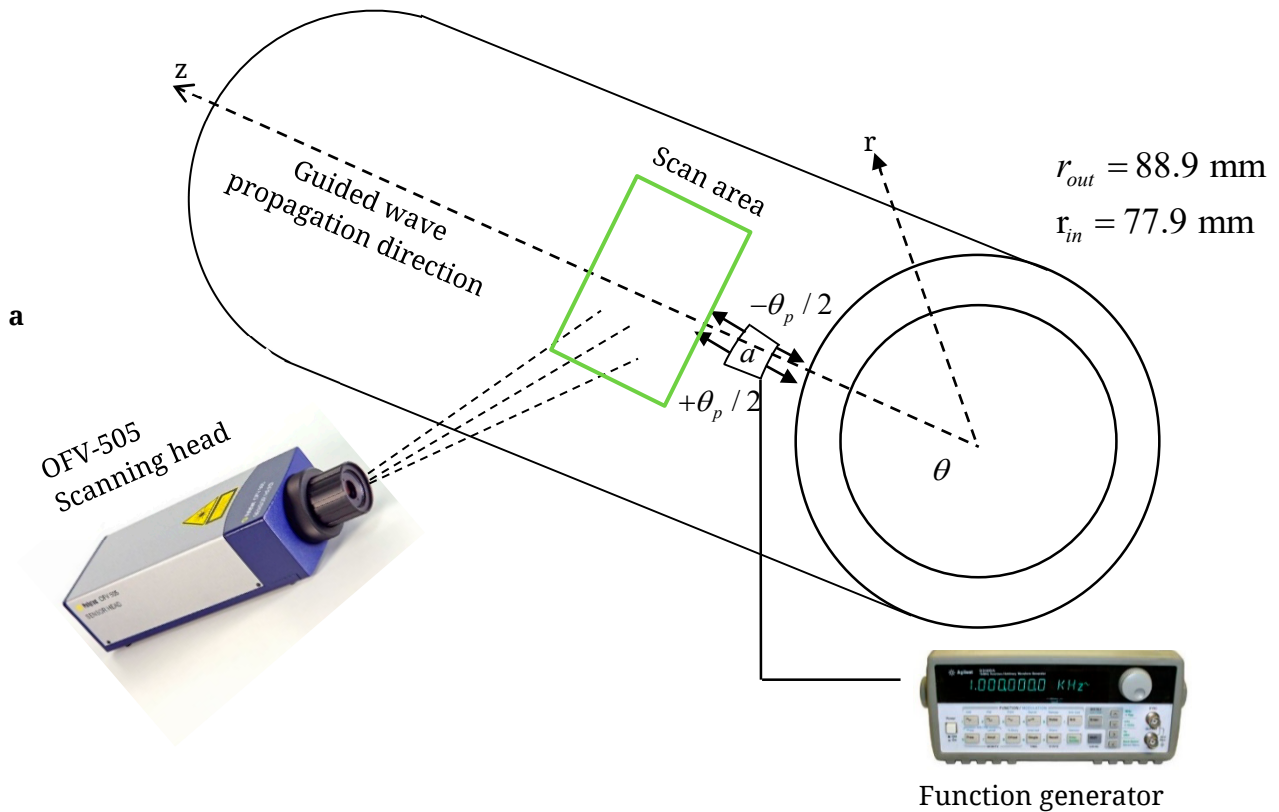

Figure 16. Instrumentation used for measurement of out of plane velocity measurement in the "6-inch schedule 40" pipe due to PWAS excitation.
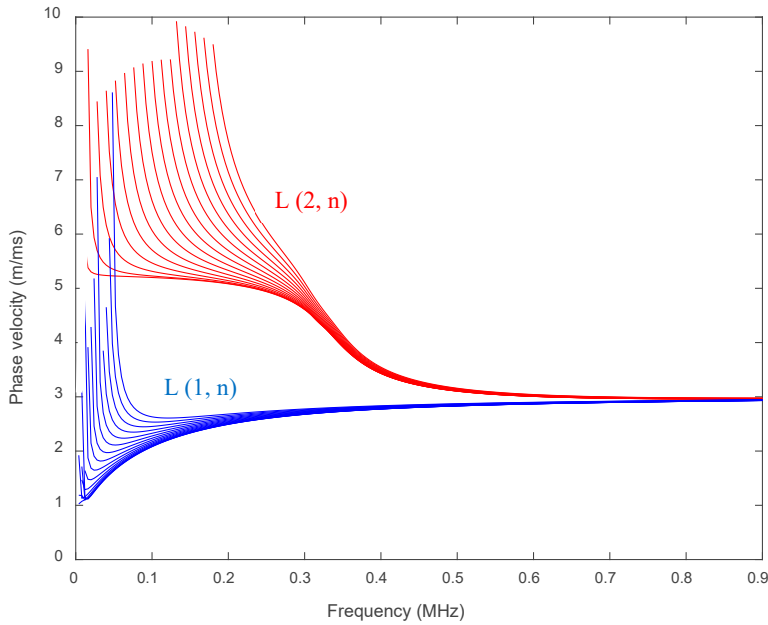
Figure 17. Dispersion curve of "6-inch schedule 40" pipe using the SAFE approach. The dispersion curves are generated for L(1,n) and L(2,n).
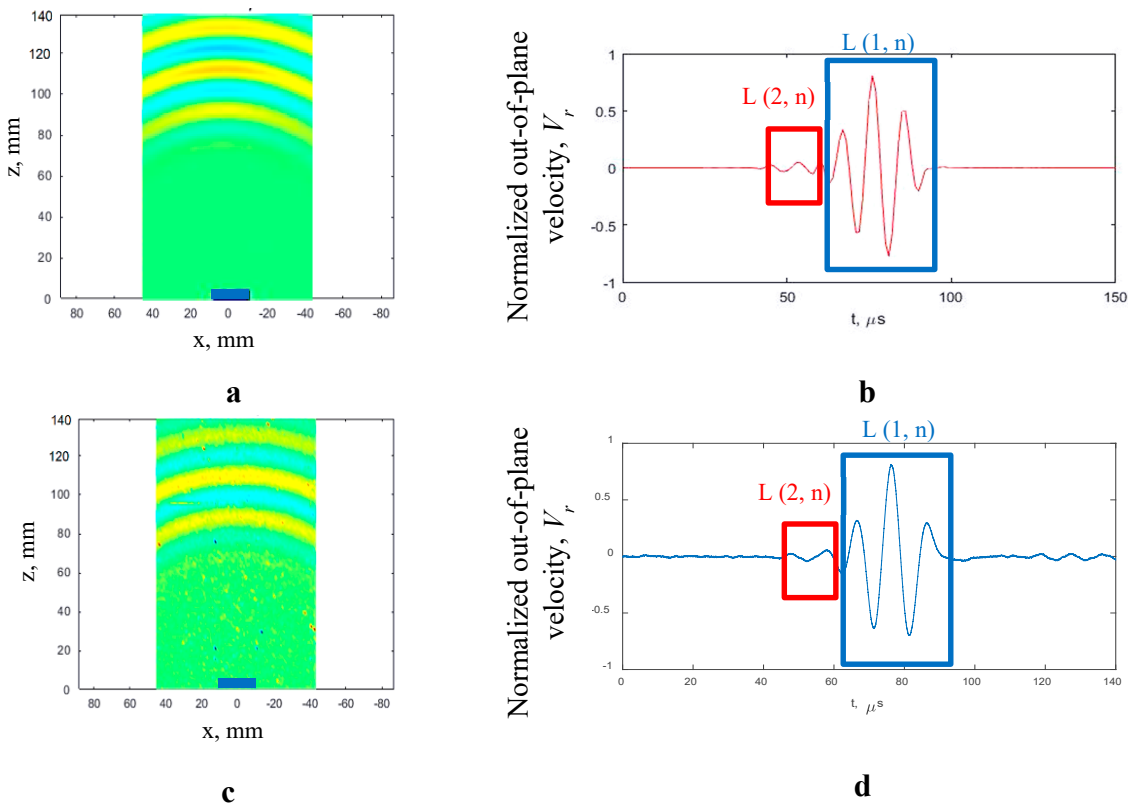

Figure 18. Comparison of experimental with SAFE- NME predictions. (**a**) Simulation of longitudinal guided wave propagation in "6-inch schedule 40" pipe due to PWAS excitation. (**b**) Out of plane velocity predictions at a distance of 150 mm from PWAS. (**c**) SLDV measurement of guided wave propagation in "6-inch schedule 40" pipe. (**d**) Out of plane velocity measurements at a distance of 150 mm from PWAS using SLDV.

Factors Affecting the Convergence of Complete Analytical Model Simulation

Excitation frequency

One of the major deciding factors for convergence of analytical model simulation is the frequency of excitation. Certain non-axisymmetric modes do not exist, or the contribution may be poor, depending on the tone burst central frequency due to the cut off frequency of that particular mode. Hence the significance of that particular mode will be poor in normal mode expansion.

Normal mode expansion coefficient

Another important deciding factor for convergence of analytical model prediction is the relative amplitude factors of the various circumferential order modes. If the relative amplitude factor of a higher-order non-axisymmetric mode is very low compared to axisymmetric as well as the first few non-axisymmetric modes, those modes do not contribute considerably to the predictions. The relative amplitude factor for the multi-layer cylinder considered in Section "**Dispersion curves**" is presented in Figure 7. The coefficients post "$n \sim> 40$" are smaller compared to "$n \sim< 40$". We also observe some nonaxisymmetric modes are not excited or have zero amplitude (mode-rejection). The trend of nonaxisymmetric mode amplitude and the mode-rejection depends on the dimension of the PWAS.

SUMMARY, CONCLUSIONS, AND FUTURE WORK

Summary

Guided wave propagation in multilayered hollow cylinders, for a localized excitation, such as PWAS excitation, consists of axisymmetric and non-axisymmetric hollow cylinder guided wave modes. In this research, the SAFE approach is used for obtaining axisymmetric as well as non-axisymmetric guided waves in a multilayer hollow cylinder. Non-axisymmetric hollow cylinder modes possess a higher number of circumferential nodes with an increase in the order of non-axisymmetry, which helps to predict the guided wave propagation due to a non-axisymmetric excitation. The theoretical equation of finite size PWAS excitation on a multilayer hollow cylinder was developed using the novel SAFE-normal mode expansion method. The complete analytical model developed was used for predictive modeling of guided wave propagation in a multilayer hollow cylinder. Predictive modeling of guided wave propagation in the multilayer hollow cylinder was also performed by using a novel wrapped plate approximation method. A comparison of the complete analytical model for hollow cylinder guided wave propagation and the wrapped plate approximation was performed, and a good match was observed for the dimension of the multilayer hollow cylinder under

consideration. Experimental validation of the theoretical development was also achieved in this paper. A "6-inch schedule-40" pipe was excited with PWAS, and the guided wave propagation area scan was performed by using SLDV. Complete analytical model guided wave prediction due to PWAS excitation was compared with experimental observation, and a close match of prediction and experiment was observed.

Conclusions

The present complete analytical model developed for predictive guided wave propagation due to a finite size PWAS transducer excitation showed a good match compared to the experimental measurements. Finite-size PWAS excitation excites axisymmetric as well as nonaxisymmetric hollow cylinder guided wave modes. Many nonaxisymmetric guided wave modes need to be included in the solution in the case of such a finite-size transducer excitation source for accurate prediction of guided wave modes. The contribution of nonaxisymmetric guided wave modes in the complete solution in each mode-family depends on the finite-size of the transducer. The simplified Lamb wave approximation of hollow cylinder guided wave propagation proposed in the present research is a good method for wave propagation prediction in low curvature multi-layered cylinder to avoid complexity due to non-axisymmetric hollow cylinder mode.

Future Work

An immediate extension of this work would be, a complete solution of PWAS excitation hollow cylinders by adding circumferential Lamb type (CLT) mode also in the simulation. The present manuscript did not discuss the improvements in the method, which can be obtained by improvements in the SAFE meshing methodology to make the computation more efficient and fast [32,33]. The proposed method can be improved by using efficient SAFE-meshing methods.

AUTHOR CONTRIBUTIONS

In this article, the formal analysis was done by RJ. The detailed methodology was provided by RJ, LY and VG. RJ prepared the original draft; review and editing were done by RJ, LY and VG.

CONFLICTS OF INTEREST

The authors declare no conflict of interest.

REFERENCES

1. Rose JL. Ultrasonic Guided Waves in Solid Media. Cambridge (UK): Cambridge University Press; 2014.

2. Gazis DC. Exact Analysis of the Plane-strain Vibrations of Thick-walled Hollow Cylinders. J Acoust Soc Am. 1958;30:786-94.

3. Ditri JJ, Rose JL. Excitation of guided elastic wave modes in hollow cylinders by applied surface tractions. J Appl Phys. 1992;72(7):2589-97.

4. Li J, Rose JL. Excitation and propagation of non-axisymmetric guided waves in a hollow cylinder. J Acoust Soc Am. 2001;109(2):457-64,.

5. Sun Z, Zhang L, Rose JL. Flexural Torsional Guided Wave Mechanics and Focusing in Pipe. J Press Vessel Technol. 2005;127(4):471.

6. Quarry MJ, Rose JL. Multimode Guided Wave Inspection of Piping Using Comb Transducers. Mater Eval. 1999;57(10):1089-90.

7. Alleyne DN, Cawley P. Long Range Propagation of Lamb Waves in Chemical Plant Pipework. Mater Eval. 1997;45(4):504-8.

8. Alleyne DN, Cawley P. The excitation of Lamb Waves in Pipes Using Dry-coupled Piezoelectric Transducers. J Nondestruct Eval. 1996;15(1):11–20.

9. Li F, Liu Z, Sun X, Li H, Meng G. Propagation of guided waves in pressure vessel. Wave Motion. 2015;52:216-28.

10. Sause MGR, Hamstad MA, Horn S. Finite element modeling of lamb wave propagation in anisotropic hybrid materials. Compos Part B Eng. 2013;53:249-57.

11. Tschöke K, Gravenkamp H. On the numerical convergence and performance of different spatial discretization techniques for transient elastodynamic wave propagation problems. Wave Motion. 2018;82:62-85.

12. Willberg C, Duczek S, Vivar Perez JM, Schmicker D, Gabbert U. Comparison of different higher order finite element schemes for the simulation of Lamb waves. Comput Methods Appl Mech Eng. 2012;241-244:246-61.

13. Hayashi T, Kawashima K, Sun Z, Rose JL. Analysis of flexural mode focusing by a semianalytical finite element method. J Acoust Soc Am. 2003;113(3):1241-8.

14. Dong SB, Nelson RB. On Natural Vibrations and Waves in Laminated Orthotopic Plates. J Appl Mech. 1972;39(3):739-45.

15. Huang KH, Dong SB. Propagating waves and edge vibrations in anisotropic composite cylinders. J Sound Vib. 1984;96(3):363-79.

16. Dong SB, Huang KH. Edge vibrations in laminated composite plates. J Appl Mech. 1985;41:322-7.

17. Hladky-Hennion AC. Finite element analysis of the propagation of acoustic waves in waveguides. J Sound Vib. 1996;194(2):119-36.

18. Gavrić L. Computation of propagative waves in free rail using a finite element technique. J Sound Vib. 1995;185(3):531-43.

19. Han X, Liu GR, Xi ZC, Lam KY. Characteristics of waves in a functionally graded cylinder. Int J Numer Methods Eng. 2002;53(3):653-76.

20. Liu GR, Dai KY, Han X, Ohyoshi T. Dispersion of waves and characteristic wave surfaces in functionally graded piezoelectric plates. J Sound Vib. 2003;268(1):131-47.

21. Taciroglu E, Liu CW, Dong SB, Chun CK. Analysis of laminated piezoelectric circular cylinders under axisymmetric mechanical and electrical loads with

a semi-analytic finite element method. Int J Solids Struct. 2004;41(18-19):5185-208.

22. Finnveden S. Evaluation of modal density and group velocity by a finite element method. J Sound Vib. 2004;273(1-2):51-75.

23. Bartoli I, Marzani A, Lanza di Scalea F, Viola E. Modeling wave propagation in damped waveguides of arbitrary cross-section. J Sound Vib. 2006;295(3-5):685-707.

24. Marzani A, Viola E, Bartoli I, Lanza di Scalea F, Rizzo P. A semi-analytical finite element formulation for modeling stress wave propagation in axisymmetric damped waveguides. J Sound Vib. 2008;318(3):488-505.

25. Perez JMV, Eisenträger S, Gabbert U. Analytical and higher order finite element hybrid approach for an efficient simulation of ultrasonic guided waves I: 2D-analysis. Smart Struct Syst. 2014;13(4):587-614.

26. Shen Y, Giurgiutiu V. Combined analytical FEM approach for efficient simulation of Lamb wave damage detection. Ultrasonics. 2016;69:116-28.

27. Bhuiyan MY, Shen Y, Giurgiutiu V. Guidedwave based crack detection in the rivet hole using global analytical with local FEM approach. Materials. 2016;9:7.

28. Kamal AM, Lin B, Giurgiutiu V. Exact analytical modeling of power and energy for multimode lamb waves excited by piezoelectric wafer active sensors. J Intell Mater Syst Struct. 2014;25(4):452-71.

29. Lin B, Gresil M, Cuc A, Giurgiutiu V. Predictive modeling of piezoelectric wafer active sensors for structural health monitoring. Ferroelectrics. 2014;470(1):168-82.

30. Shen Y, Giurgiutiu V. WaveFormRevealer: An analytical framework and predictive tool for the simulation of multi-modal guided wave propagation and interaction with damage. Struct Heal Monit. 2014;13(5):491-511.

31. Giurgiutiu V. Structural health monitoring with piezoelectric wafer active sensors. 2nd ed. Waltham (MA, US): Elsevier Academic Press; 2014.

32. Raghavan A, Cesnik CES. Finite-dimensional piezoelectric transducer modeling for guided wave based structural health monitoring. Smart Mater Struct. 2005;14(6):1448-61.

33. Barouni AK, Saravanos DA. A layerwise semi-analytical method for modeling guided wave propagation in laminated composite infinite plates with induced surface excitation. Wave Motion. 2017;68:56-77.

34. Mei H, Giurgiutiu V. Guided wave excitation and propagation in damped composite plates. Struct Heal Monit. 2018;18(3):690-714.